The influence of phosphorus and Mo loading on the MoS_2 phase morphology and performance of sulfided Mo/Al_2O_3 catalysts in HDO of rapeseed oil

EVGENIYA N. VLASOVA [a,b], VERA P. PAKHARUKOVA [a], GALINA A. BUKHTIYAROVA[a,b], IRINA V. DELIY [a,b], PAVEL V. ALEKSANDROV [a,b], ALEKSANDER A. PORSIN, EVGENY YU. GERASIMOV[a,b], VALERII I. BUKHTIYAROV[a,b]
[a] – Boreskov Institute of Catalysis SB RAS, 630090, Pr. Lavrentieva 5, Novosibirsk, RUSSIA.
[b] – Novosibirsk National Research University, 630090, Pirogova Street 2, Novosibirsk, RUSSIA
evgenia@catalysis.ru

Abstract: - The effect of Mo loading on the dispersion of sulfide phase and catalytic activity of MoS_2/Al_2O_3 catalysts in the rapeseed HDO was studied. Five catalysts with Mo loading between 10 and 16 wt.% were prepared by impregnation of alumina with aqueous solutions containing MoO_3, H_3PO_4 and citric acid, subsequent drying and high-pressure sulfidation. HDO activity of the MoS_2/Al_2O_3 catalysts was enhanced with the Mo content increase from 10 to 12 wt.% and then was decreased with the further increase of Mo loading. The behavior of MoS_2/Al_2O_3 and P-MoS_2/Al_2O_3 catalysts with the same Mo loading (near 14 wt.%) was compared in the hydrodeoxygenation of rapeseed oil demonstrating the higher activity of P-promoted system. The modeling of XRD patterns with using of the Debye Function Analysis (DFA) gives the lower d_{XRD} of the MoS_2 particles in the P-MoS_2/Al_2O_3 catalyst in comparison with MoS_2/Al_2O_3 one. We proposed that P incorporation in the MoS_2 slabs can result in a higher deformation of the supported MoS_2 particles, which in turn could have been a reason of higher activity of P-MoS_2/Al_2O_3 catalyst.

Key-Words: - hydrotreatment, hydrodeoxygenation, MoS_2, sulfide catalyst, rapeseed oil, co-processing

1 Introduction

The development of new catalytic processes for the production of liquid motor fuels from the renewables is stimulated by the growing demand for transportation fuels along with the decrease in oil reserves and vital tendency to reduce the greenhouse gas emissions. The hydroprocessing of triglyceride-based feedstock, namely vegetable oils, waste cooking oil, animal fats, etc., produces the mixture of C_{12}-C_{18} alkanes, which are the valuable components of the petroleum-based motor fuels [1]. The conventional hydrotreating catalysts ($CoMo/Al_2O_3$ or $NiMo/Al_2O_3$) are widely used for the hydrodeoxygenation (HDO) of triglyceride-based feedstocks [2-5] or their mixture with petroleum-derived fractions [5-11].

2 Problem Formulation

The HDO of triglycerides over sulfide $Co(Ni)Mo/Al_2O_3$ catalysts proceeds through the so-called direct deoxygenation route producing water or via decarbonylation pathway, giving CO among the final products along with alkanes [12,13]. The production of CO and CO_2 in the HDO processes is highly is highly undesirable because of several ecological and technological reasons [4,5]. The conversion of triglycerides via decarbonylation reaction led to decrease in the yield of the liquid products and could cause the formation of CH_4 and CO_2 via the hydrogenation or the water gas shift reaction. CO_2 in the presence of water can form carbonic acid and causes corrosion of the equipment. The accumulation of CH_4 and CO in the recycle gas would decrease the partial pressure of hydrogen, which is the critical parameter for the production of sulfur-free motor fuels from the mixture of petroleum oil with triglyceride-based feedstock [14]. The activity of a $CoMo/Al_2O_3$ catalyst in hydrodesulfurization reactions of diesel fractions decreases in the presence of triglyceride feedstock [15–17], presumably, as a result of inhibition of HDS and HDN reactions with carbon monoxide [17,18]. The non-promoted sulfide Mo/Al_2O_3 catalysts were shown to provide RSO conversion without considerable COx formation [19-21], that makes them the promising candidates for the HDO of triglycerides. Recently, the dual-bed catalytic system consisting of MoS_2/Al_2O_3 and $Co–MoS_2/Al_2O_3$ catalysts is proposed for the production of ULSD from a straight-run gas oil mixed with rapeseed oil (10–45 wt %). The

conversion of rapeseed oil to alkanes proceeds in the bed of MoS_2/Al_2O_3 catalyst via the route of "direct" hydrodeoxygenation without the formation of carbon oxides, while the HDS of gas oil occurs in the bed of the $Co–MoS_2/Al_2O_3$ hydrotreating catalyst [22]. So, the use of MoS_2/Al_2O_3 catalyst for the HDO of triglycerides or for the HDT of triglycerides/SRGO mixture aids avoiding a technological problems, increasing the yield of diesel fuel, preventing greenhouse gases formation (CH_4, CO, CO_2).

The effect preparation conditions on the morphology of MoS_2 slabs and the HDS performance of MoS_2/Al_2O_3 catalyst were thoroughly investigated [23-26], while there are no similar investigations concerning HDO reactions. In our work the effect of Mo loading and phosphor on the performance of MoS_2/Al_2O_3 catalysts in HDO of rapeseed oil was investigated. Catalysts were prepared by an impregnation method with or without addition of phosphoric acid in the impregnation solution, prepared from MoO_3 and citric acid.

3 Problem Solution

3.1 Experimental

Mo/Al_2O_3 catalysts were prepared by impregnation of alumina granules (BET surface area 208 $m^2\ g^{-1}$, pore volume 0.68 ml g^{-1}, average pore diameter 13,2 nm, purchased by JSK "Promkataliz", Ryazan, Russia) with aqua solutions containing citric acid, H_3PO_4 and different amount of MoO_3, (all purchased by Vekton, Russia). The catalyst designation and chemical composition are given in Table 1. To investigate the influence of phosphorus addition sample "HDO-6" was prepared without the addition of phosphoric acid to impregnation solution. The catalysts were dried in nitrogen flow at room temperature and then at 110°C for 4 h.

Table 1. The chemical composition of the catalysts

Designation	Mo, wt%	P, wt.%
HDO-1	10.1	1.6
HDO-2	11.0	1.5
HDO-3	12.4	1.7
HDO-4	13.9	1.6
HDO-5	16.0	2.3
HDO-6	13.8	0

The textural properties of the catalysts were determined using nitrogen physisorption with an ASAP 2400 instrument (USA); the elemental analysis was performed using Optima 4300 DV (Perkin Elmer, France). The morphology of sulfide phase was studied using a JEM-2010 electron microscope (JEOL, Japan) with 1.4 Å lattice resolution at a 200 kV accelerating potential. Prior to the study, the samples were ground, suspended in ethanol and placed on a copper grid coated with a holey carbon film. XRD investigations were carried out at an ARL X'TRA diffractometer (Thermo, Switzerland) with a Si(Li) solid-state detector and Cu K_α radiation. The measurements were carried out in the 2θ range of 10°-80° with a step of 0.1°. Phase analysis was performed using the ICDD PDF-2 database.

The catalytic experiments were performed in a trickle-bed down-flow reactor with an inner diameter of 16 mm and length of 570 mm. In each experiment 10 ml of catalyst (full-sized granules) was diluted by an inert material, carborundum (0.1–0.25 mm size fraction) in a 1:2 volume ratio [27]. The catalysts were examined after sulfidation with straight-run gas oil containing additionally 0.6 wt. % sulfur as dimethyl disulfide (at H_2 pressure 3.5 MPa; H/C – 300 Nm^3/m^3; LHSV- 2 $hour^{-1}$). The sulfidation was performed at 340°C during 6 h (heating rate was 25°C in hour). The catalytic experiments were performed at H_2 pressure 4.0 MPa, H/C – 600 Nm^3/m^3; LHSV – 1.5 h^{-1}, temperature – 260, 280, 300, 320 and 340°C; using mixture of 20 wt.% of rapeseed oil (RSO) diluted with straight run gas oil (SRGO). Properties of mixture were d = 0.86 g/cm^3, 2.34 wt. % O, 0.82 wt% S, 141 ppm N. The duration of each stages differing in temperature was 12 h; the residual sulfur and oxygen contents were obtained by averaging the data for three samples taken through 10, 11 and 12 h after the beginning of the current stage.

The sulfur content of the feedstock and that of the hydrogenated products were measured on a Lab-X 3500SCl energy dispersive X-ray fluorescence analyzer (Oxford Instruments, United Kingdom). The total oxygen content of the reaction mixture before and after reaction was determined using a Vario EL Cube CHNSO analyzer (Elementar Analysensysteme GmbH, Germany).

The contents of C_{18} and C_{17} alkane (the products of RSO hydrodeoxygenation) in the products were evaluated using two-dimensional gas chromatography (Agilent 7890A GC equipped with a flame-ionization detector and an Agilent flow modulator). In the first dimension, separation was fulfilled using helium as carrier gas and ZB-WAX capillary column of 25 m long with a diameter of 0.25 mm and the film thickness of 0.25 μm (Phenomenex, United States). An HP-5 column of 5 m long and 0.25 mm in diameter with a film

thickness of 0.25 μm (Agilent, United States) was used for the separation of components in the second dimension. The carrier gas was hydrogen. The conditions of analysis were 70°C for 0.5 m in, 8°C/min, and 260°C for 25 min. The flow through the first column was 0.5 mL/min (helium), while the flow through the second column was 31 mL/min (hydrogen). The period of modulation was 2.2 s. The volume of the introduced sample was 0.5 μL, and the split ratio was 1:200. The chromatographic data were processed with the ChemStation (Agilent) and Image GC (Zoex) software.

Gas phase was analyzed on-line using a gas chromatograph «Chromos 1000» (Dzerzhinsk, Russia), equipped with the FID detector. The concentrations of CO and CO_2 were determined in the form of methane after separation on column packed with 80/100 mesh HayeSep® («Sigma-Aldrich», St. Louis, MO, USA) and subsequent hydrogenation over reduced Pd catalyst at 340 °C.

3.2 Results and discussion

3.2.1 Characterization of the catalysts

Crystalline phases of the molybdenum sulfide catalysts were studied by Powder X-ray diffraction (XRD) analysis and high-resolution transmission electron microscopy (HRTEM).

HRTEM images of samples HDO-1, HDO-3 and HDO-5 taken after reaction demonstrate the typical surface fragments of the sulfided MoS_2 particles (Fig.1). The HDO-1 catalyst with the lowest Mo content (10.1 wt.% of Mo) is characterized by the lowest values of average slab length (3.1 nm) and the stacking number (1.2), which are increased with the Mo loading increasing (table 2). For the catalyst HDO-5 with the loading of 16 wt.% of Mo slab length is increased to 4.2 nm, the stacking number is increased to 1.5.

Fig. 2 shows XRD patterns of the γ-Al_2O_3 support and MoS_2/γ-Al_2O_3 catalysts taken after reaction. Highly broadened peaks in the 2θ ranges of 33-35° and 58-60° were detected in the XRD patterns of the catalysts, which indicate formation of highly dispersed MoS_2 phase.

The formation of the poorly crystallized MoS_2 phase was revealed in the catalysts (JCPDS#37-1492, a=b=3.161 Å, c=12.299 Å, α=β=90°, γ=120°). Disappearance of the first (002) reflection indicates the small size of coherently scattering domain (d_{XRD}) in the [001] direction, in which the skeletal MoS_2 layers are packed.

The data obtained from HRTEM and XRD confirmed the formation of low crystalline highly dispersed MoS_2 phase.

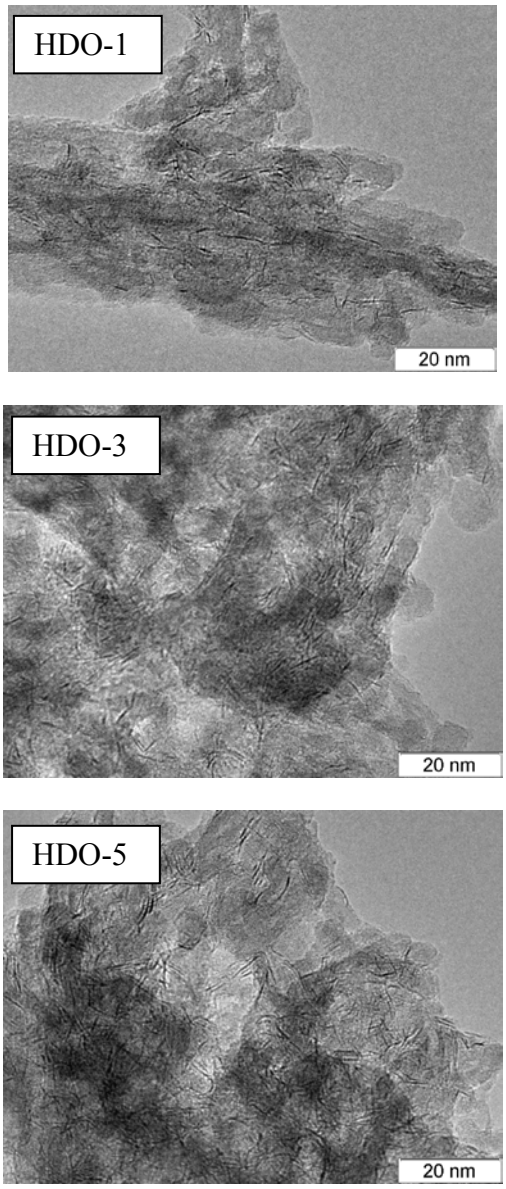

Fig.1. HRTEM images of the catalysts HDO-1 (10.1 wt.% Mo), HDO-3 (12.4 wt.% Mo), HDO-5 (16.0 wt.% Mo).

Table 2. HRTEM parameters of the sulfided catalysts

Catalyst	Average slab length (nm)	Stacking number
HDO-1	3.1	1.2
HDO-3	3.9	1.6
HDO-5	4.8	1.5

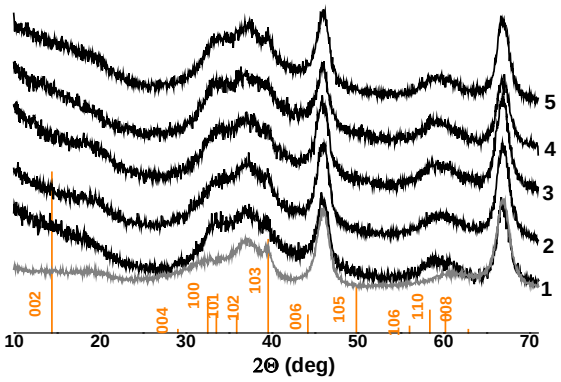

Fig.2. XRD patterns of the HDO-1 (1), HDO-2 (2), HDO-3 (3), HDO-4 (4) and HDO-5 (5) catalysts in comparison with XRD pattern of the $\gamma-Al_2O_3$ support. The peaks of the MoS_2 phase are shown.

3.2.2 Influence of Mo loading on HDO activity

Experiments were performed at the temperature range 260-340°C, H_2 pressure 4.0 MPa, H/C – 600 Nm^3/m^3; LHSV – 1.5 h^{-1}. The feed was 20 wt.% of RSO in SRGO. Complete oxygen conversion was observed at temperatures 340 and 320°C (fig.3). The lowering temperature resulted in a decrease of oxygen conversion over all catalysts (Fig.3). HDO activity of the MoS_2/Al_2O_3 catalysts was enhanced with the Mo content increase from 10 to 12.4 wt.%, HDO-3 catalyst being the most active catalyst in HDO of RSO mixed with SRGO (Fig.4). Further increase of Mo loading led to decrease of HDO activity.

It is known that non-promoted catalyst MoS_2/Al_2O_3 is less active in HDS and HDN reactions of SRGO than sulfide Co(Ni)Mo/Al_2O_3 catalysts. Temperature range of 320-340°C is enough to observe the change in HDS and HDN activities of the catalysts depending on Mo loading (Fig.5). The HDO-3 catalyst, as in the case of HDO, is the most active in HDS and HDN reactions of SRGO in presence of rapeseed oil. Such dependencies of catalytic activity on Mo loading can be explained by the change of active sites quantities along with the increase of particle sizes. At first, the overall quantities of MoS_2 edge sites, which are the active sites for the HDS and HDO reactions, are increased with Mo loading to some value. But with the increase of slab sizes caused by increase of Mo loading the quantities of MoS_2 edge sites go through the maxima and start to decrease at some value.

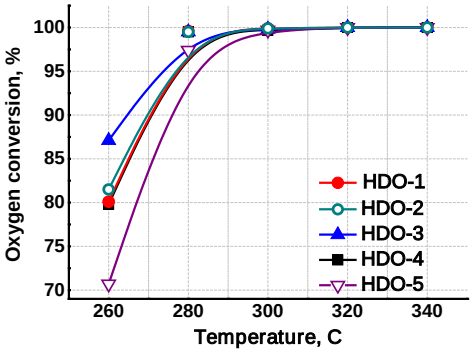

Fig.3. Dependence of oxygen conversion on the temperature over sulfide catalysts with different Mo content

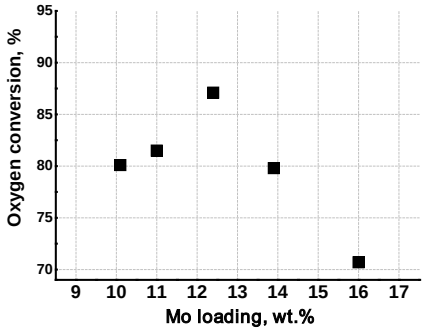

Fig.4. Dependence of oxygen conversion on Mo loading in the HDO catalysts (T-260°C, LHSV – 1.5 h^{-1}, H/C – 600 Nm^3/m^3)

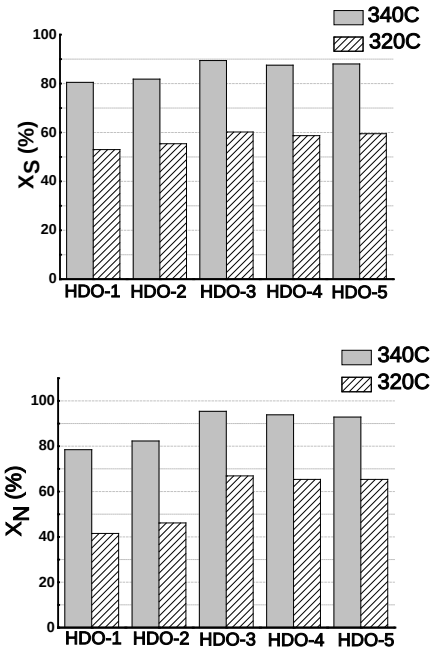

Fig.5. Dependence of sulfur and nitrogen conversions on Mo loading in the sulfide catalysts at 320 and 340°C

The selectivity of RSO conversion through HDO or HDeCO_x pathways was evaluated taking gas

phase analysis and the results of C_{18} and C_{17} content measurement by means of two-dimensional chromatography. The typical chromatograms of SRGO and reaction products, obtained during HDO of RSO/SRGO mixture over MoS_2 at 340°C is presented in Fig.6. The quantitative analysis of C_{18} and C_{17} in the reaction products and in the SRGO let us to calculate the selectivity of octadecane formation that lies within the region 97-99% for both catalysts at whole conversion of RSO (at 320 and 340°C).

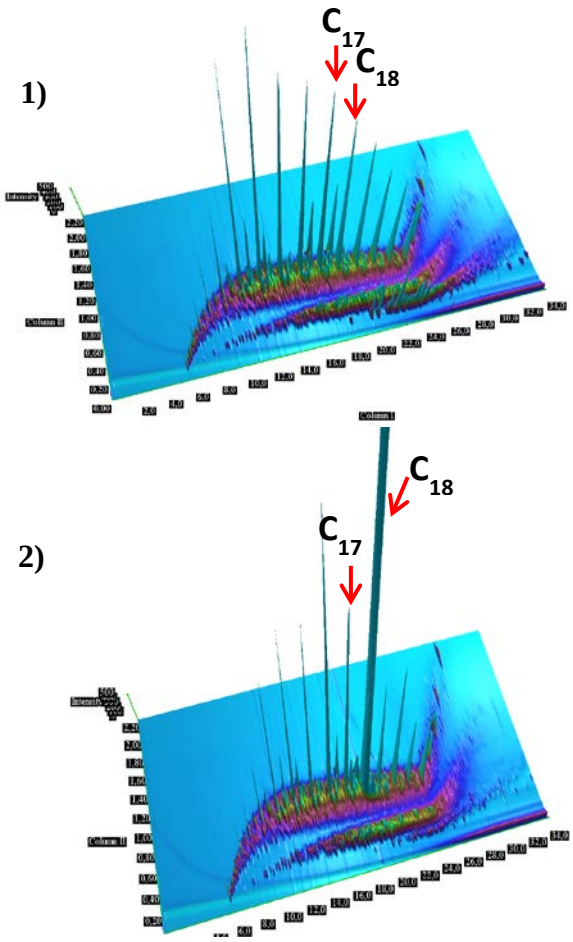

Fig.6. 2D-chromatograms of straight run gas oil (1) and the product obtained (2) in presence of P-MoS_2/Al_2O_3 at 340°C

The results of CO_x analysis in the exit gas flow confirmed the high selectivity of RSO hydrodeoxygenation though the "direct" HDO route over all catalysts. CO_x content was negligible at 260°C (about 0.04 vol.%) and slightly increased (up to 0.10-0.12 vol.%), with the temperature raising from 260 to 340°C. But the selectivity of $DeCO_x$ pathway calculated from the gas phase analysis did not exceed 3.0% even at 340°C.

3.2.3 Effect of phosphorus addition

It's known that the small crystallite size of MoS_2 in hydrotreating catalysts limits application of traditional XRD methods for structure diagnostics. The Debye Function Analysis (DFA) was used to get information about the structure of MoS_2 nanoparticles from the XRD data. The Debye Scattering Equation (DSE) allows calculating XRD pattern of model nanoparticle with taking into account the particle shape, size, chemical composition, and atomic structure [28-31]. Calculating and fitting XRD patterns were performed using the DIANNA software [32]. To evaluate an agreement between the calculated and experimental XRD profiles, a p rofile discrepancy factor (R_p) was determined.

Fig.7 shows the X-ray diffraction patterns of the γ-Al_2O_3 support and MoS_2/γ-Al_2O_3 catalysts. The XRD patterns of the catalysts exhibit the highly broadened peaks in the 2θ ranges of 33-35° and 58-60°, which indicate formation of highly dispersed MoS_2 phase. Overlapping of the diffraction lines corresponding to the MoS_2 and γ-Al_2O_3 phases complicates the analysis. So, the difference curves between the normalized XRD patterns of the catalyst and support were obtained (Fig.8). It was need to obtain information about structure of MoS_2 nanoparticles.

The formation of the poorly crystallized MoS_2 phase was revealed in the catalysts (JCPDS#37-1492, a=b=3.161 Å, c=12.299 Å, α=β=90°, γ=120°). Disappearance of the first (002) reflection indicates the small size of coherently scattering domain (d_{XRD}) in the [001] direction, in which the skeletal MoS_2 layers are packed. HRTEM data also gave evidence of poor crystallization of the MoS_2 particles along the [001] direction (Fig.9). The average stacking number of 1.6 was determined in the both P-MoS_2/Al_2O_3 and MoS_2/Al_2O_3 catalysts (Table 3).

A direct modeling of XRD patterns with using the DSE was performed to determine the average size of coherently scattering domain. Starting from one MoS_2 unit cell, a set of model plate-like crystallites was generated by varying lengths of the crystallite edges. The simulation of XRD data confirmed the absence of significant MoS_2 stacking in the P-MoS_2/Al_2O_3 and MoS_2/Al_2O_3 catalysts.

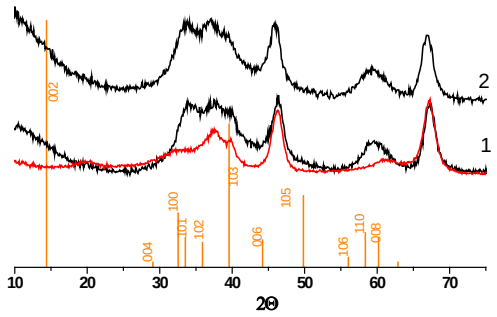

Fig.7. XRD patterns of the P-MoS_2/Al_2O_3 (1) and MoS_2/Al_2O_3 (2) catalysts in comparison with XRD pattern of the $\gamma-Al_2O_3$ support. The peaks of the MoS_2 phase are shown.

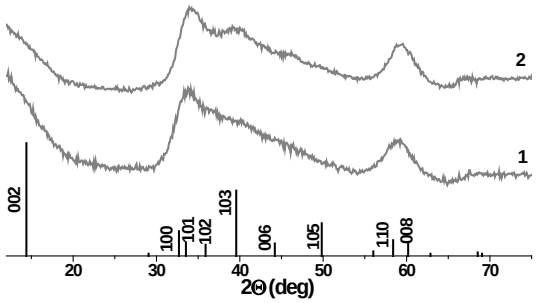

Fig.8. Difference XRD curves for the P-MoS_2/Al_2O_3 (1) and MoS_2/Al_2O_3 (2) catalysts

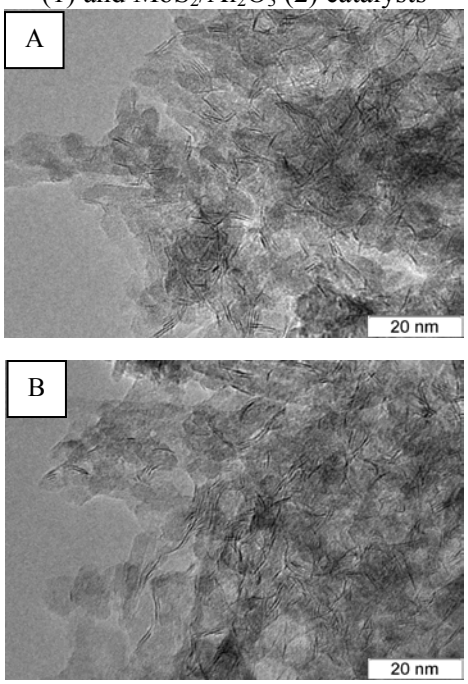

Fig.9. HRTEM images of the P-MoS_2/Al_2O_3 (A) and MoS_2/Al_2O_3 (B) catalysts

Table 3. Dispersion characteristics of MoS_2 particles in the sulfide catalysts from the XRD and HRTEM data

P-MoS_2/Al_2O_3		MoS_2/Al_2O_3	
average slab length of MoS_2 crystallites according to the XRD data modeling			
d_{XRD} (nm)	R_p (%)	d_{XRD} (nm)	R_p (%)
2.2x2.2	8.3	2.5x2.5	9.0
2.5x2.5	7.7	2.8x2.8	8.5
2.8x2.8	8.2	3.2x3.2	7.9
		3.5x3.5	7.8
		3.8x3.8	8.6
average slab length of MoS_2 particles according to the HRTEM data			
4.6		4.9	
average stacking number according to the HRTEM data			
1.6		1.6	

Fig.10 shows the experimental difference XRD curve of the P-MoS_2/Al_2O_3 catalyst in comparison with calculated XRD patterns for the plate-like MoS_2 crystallites containing one and two MoS_2 layers with lateral dimensions of 2.5x2.5 nm (MoS_2 crystallites composed of 8x8x0.5 and 8x8x1 unit cells, respectively).

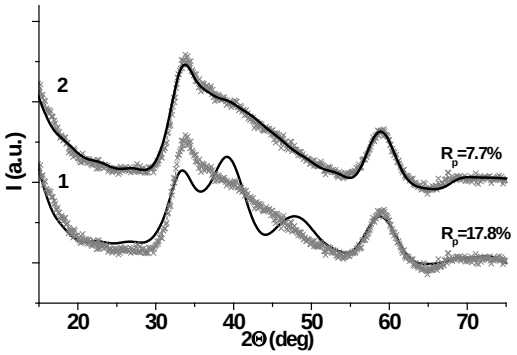

Fig.10. Experimental difference XRD curve of the P-MoS_2/Al_2O_3 catalyst and calculated XRD patterns for MoS_2 crystallites with dimensions of 2.5x2.5x1.2 nm (1) and 2.5x2.5x0.6 nm (2), containing one and two layers along the [001] direction, respectively.

The model of one-layer thick crystallites is more appropriate for describing the experimental XRD pattern. The calculated XRD pattern for the MoS_2 crystallites composed of two layers differs drastically from the experimental one. The lateral dimensions of MoS_2 crystallites of one-layer thickness (slab length) in the P-MoS_2/Al_2O_3 and MoS_2/Al_2O_3 catalysts were refined. The sizes d_{XRD} and corresponding discrepancy factors R_p are listed in Table 3.

The obtained data show that MoS_2 particles in the P-MoS_2/Al_2O_3 catalyst are characterized by a lower average size of coherently scattering domain d_{XRD}. The best fitting results were obtained at the slab sizes of 2.5 and 3.2-3.5 nm for P-MoS_2/Al_2O_3 and MoS_2/Al_2O_3 catalysts, respectively. A comparison of the particle sizes evaluated from XRD and HRTEM data shows a pronounced discrepancy. The dimensions of the coherent scattering domains determined from XRD data are significantly smaller than slab length of MoS_2 determined from HRTEM data (Table 3). The discrepancy is explained by deformation of MoS_2 particles, which leads to breaking coherence. Indeed, the MoS_2 sheets observed in the HRTEM images are curved or folded (Fig. 9). A lower value of d_{XRD} in the case of P-MoS_2/Al_2O_3 catalyst seems to result from a higher degree of deformation of the supported MoS_2 particles. According to [33] the blending of MoS_2 slabs could led to the creation of new active sites for thiophene HDS on their basal planes.

The results of catalytic tests of the MoS_2/Al_2O_3 and P-MoS_2/Al_2O_3 catalysts in the hydrotreating of RSO/SRGO mixture are presented in the Fig.11-12. Degree of RSO hydrodeoxygenation (Fig.11) was calculated using oxygen content in the raw material (mixture of RSO with SRGO) and in the liquid products measured by means of Vario EL Cube analyzer. The RSO conversion achieved 100% at 320 and 340°C over both catalysts; but P-MoS_2/Al_2O_3 catalyst demonstrated higher HDO activity at 260, 280 a nd 300°C (Fig.11). P-MoS_2/Al_2O_3 catalyst as well displayed higher activity in HDS of SRGO in comparison with MoS_2/Al_2O_3 catalyst in the whole temperature range (Fig.12).

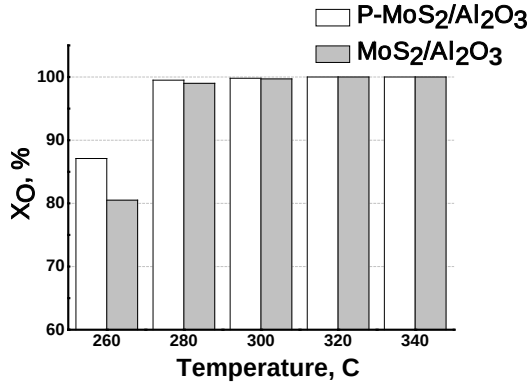

Fig.11. Hydrodeoxygenation activity of P-MoS_2/Al_2O_3 and MoS_2/Al_2O_3 catalysts at different temperatures

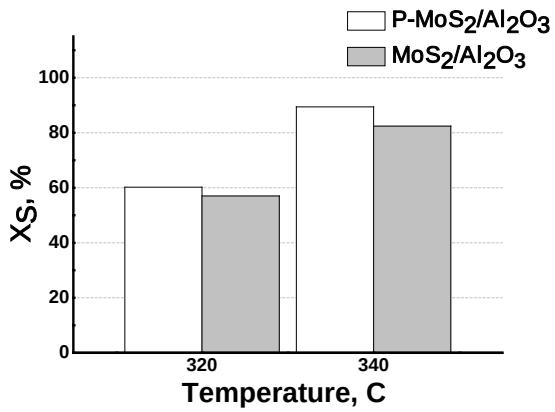

Fig.12. Hydrodesulfurization activity of P-MoS_2/Al_2O_3 and MoS_2/Al_2O_3 catalysts at 320 and 340°C

4 Conclusion

The effect of phosphorus addition on t he morphology of MoS_2 slabs and catalytic performance of sulfide Mo/Al_2O_3 catalysts in the HDO of rapeseed oil was also studied. MoS_2/Al_2O_3 catalyst was obtained by the impregnation of alumina with water solution obtained from MoO_3 and citric acid; during P-MoS_2/Al_2O_3 catalyst preparation H_3PO_4 was added to the same solution. The investigation of the sulfide MoS_2/Al_2O_3 and P-MoS_2/Al_2O_3 catalysts with XRD methods accompanied with Debye Function Analysis led us to conclusion, that sulfide particles in the P-MoS_2/Al_2O_3 catalysts are characterized by a l ower average size of coherently scattering domain d_{XRD}. A lower value of d_{XRD} in the case of P-MoS_2/Al_2O_3 catalyst seems to result from a h igher degree of deformation of MoS_2 slabs, which in turn could have been a reason of higher activity of P-MoS_2/Al_2O_3 catalyst in HDO and HDS reactions.

The effect of Mo loading on the dispersion of sulfide phase and catalytic activity of P-MoS_2/Al_2O_3 catalysts in the rapeseed HDO was also studied. With the increase of Mo loading the activities of P-MoS_2/Al_2O_3 catalysts in HDO, HDS and HDN reactions go through the maxima with the optimum Mo content – 12.4 wt%. The most probable reason of such dependencies is the coinciding change of the overall quantities of MoS_2 edge sites that is caused by the increase of sizes of MoS_2 slabs.

Acknowledgments

The authors would like to thank Dr. Patrushev Yu.V. for analysis and characterization of the products using two-dimensional gas chromatography.

The work was supported by the Ministry of Education and Science of the Russian Federation,

project № 14.575.21.0128, unique identification number RFMEFI57517X0128.

References:

[1] Gosselink R. W., Hollak S. A., Chang S. W., Reaction pathways for the deoxygenation of vegetable oils and related model compounds, *ChemSusChem*, Vol.6., No.9, 2013, pp. 15 76-1594.

[2] Vásquez M. C., Silva E. E., Castillo E. F., Hydrotreatment of vegetable oils: A review of the technologies and its developments for jet biofuel production, *Biomass and Bioenergy*, Vol.105, 2017, pp. 197-206.

[3] Melero J.A., Iglesias J., Garcia A., Biomass as renewable feedstock in standard refinery units. Feasibility, opportunities and challenges, *Energy & Environmental Science*, Vol.5, 2012, pp. 7393-7420.

[4] Furimsky E., Hydroprocessing challenges in biofuels production, *Catalysis Today*, Vol.217, 2013, pp. 13-56.

[5] Kubicka D., Tucas V. *Advances in Chemical Engeneering*, Elsevier, Vol.42, 2013.

[6] Rana B.S., Kumar R., Tiwari R., Kumar R., Joshi R.K., Garg M.O., et al., Transportation fuels from co-processing of waste vegetable oil and gas oil mixtures, *Biomass & Bioenergy*, Vol.56, 2013, pp. 43-52.

[7] Huber G.W., Corma A., Synergies between bio- and oil refineries for the production of fuels from biomass, *Angewandte Chemie-International Edition*, Vol.46, 2007, pp. 7184-7201.

[8] Al-Sabawi M., Chen J. W., Hydroprocessing of Biomass-Derived Oils and Their Blends with Petroleum Feedstocks: A Review, *Energy Fuels*, Vol.26, 2012, pp. 5373-5399.

[9] Toth C., Baladincz P., Kovacs S., Hancsok J., Producing clean diesel fuel by co-hydrogenation of vegetable oil with gas oil, *Clean Technologies and Environmental Policy*, Vol.13, 2011, pp. 581-585.

[10] Templis C., Vonortas A., Sebos I., Papayannakoset N., Vegetable oil effect on gasoil HDS in their catalytic co-hydroprocessing, *Appled Catalysis B – Environmental*, Vol.104, 2011, pp. 324-329.

[11] Sebos I., Matsoukas A., Apostolopoulos V., Papayannakoset N., Catalytic hydroprocessing of cottonseed oil in petroleum diesel mixtures for production of renewable diesel, *Fuel*, Vol.88, 2009, pp. 145-149.

[12] Kubicka D., Kaluza L., Deoxygenation of vegetable oils over sulfided Ni, Mo and NiMo catalysts, *Applied Catalysis A: General*, Vol.372, No.2, 2010, pp. 199-208.

[13] Huber G. W., O'Connor P., Corma A., Processing biomass in conventional oil refineries: Production of high quality diesel by hydrotreating vegetable oils in heavy vacuum oil mixtures, *Applied Catalysis A: General,* Vol.329, 2007, pp. 120-129.

[14] Stanislaus A., Marafi A., Rana M. S., Recent advances in the science and technology of ultra-low sulfur diesel (ULSD) production, *Catalysis today*, Vol.153, No. 1-2, 2010, pp. 1-68.

[15] Vlasova E. N., Deliy I. V., Nuzhdin A. L., Aleksandrov P. V., Gerasimov E. Y., Aleshina, G. I., Bukhtiyarova, G. A., Catalytic properties of $CoMo/Al_2O_3$ sulfide catalysts in the hydrorefining of straight-run diesel fraction mixed with rapeseed oil, *Kinetics and Catalysis*, Vol.55. No.4, 2014, pp. 481-491.

[16] Nikul'shin P. A., Sal'nikov V. A., Pimerzin A. A., Eremina Y. V., Koklyukhin A. S., Tsvetkov V. S., Pimerzin A. A., Co-hydrotreating of straight-run diesel fraction and vegetable oil on $Co(Ni)-PMo/Al_2O_3$ catalysts. *Petroleum Chemistry*, Vol.56, No.1, 2016, pp. 56-61.

[17] Bezergianni S., Dagonikou V., Sklari S., The suspending role of H_2O and CO on c atalytic hydrotreatment of gas-oil; myth or reality?, *Fuel Processing Technology*, Vol.144, 2016, pp. 20-26.

[18] Pelardy F., Daudin A., Devers E., Dupont C., Raybaud, P., Brunet S., Deep HDS of FCC gasoline over alumina supported CoMoS catalyst: Inhibiting effects of carbon monoxide and water, Applied Catalysis B: Environmental, Vol.183, 2016, pp.317-327.

[19] Kubicka D., Kaluza L., Deoxygenation of vegetable oils over sulfided Ni, Mo and NiMo catalysts, *Applied Catalysis A: General*, Vol.372, No.2, 2010, pp. 199-208.

[20] De Brimont M. R. et al., Deoxygenation mechanisms on Ni-promoted MoS_2 bulk catalysts: a c ombined experimental and theoretical study, *Journal of Catalysis,* Vol.286, 2012, pp. 153-164.

[21] Deliy I. V. et al., Hydrodeoxygenation of methyl palmitate over sulfided Mo/Al_2O_3, $CoMo/Al_2O_3$ and $NiMo/Al_2O_3$ catalysts, *RSC Advances*, Vol.4, No.5, 2014, pp. 2242-2250.

[22] Vlasova E. N., Deliy I. V., Gerasimov E. Y., Aleksandrov P. V., Nuzhdin A. L., Aleshina G. I., Bukhtiyarova G. A., Use of a Dual-Bed System for Producing Diesel Fuel from a

Mixture of Straight-Run Diesel and Rapeseed Oil over Sulfide Catalysts, *Petroleum Chemistry*, Vol.57, No.12, 2017, pp. 1156-1160.

[23] Bergwerff J. A., Jansen M., Visser T., de Jong K. P., Weckhuysen B. M., Influence of the preparation method on the hydrotreating activity of MoS_2/Al_2O_3 extrudates: A Raman microspectroscopy study on t he genesis of the active phase, *Journal of Catalysis*, Vol.243. No.2, 2006, pp. 292-302.

[24] Chen J., Oliviero L., Portier X., Maugé, F., On the morphology of MoS_2 slabs on MoS_2/Al_2O_3 catalysts: the influence of Mo loading, *RSC Advances*, Vol.5, No.99, 2015, pp.81038-81044.

[25] van Haandel L., Bremmer G. M. et al., The effect of organic additives and phosphoric acid on sulfidation and activity of $(Co)Mo/Al_2O_3$ hydrodesulfurization catalysts, *Journal of Catalysis*, Vol.351, 2017, pp. 95-106.

[26] Li H. F., Li M. F., et al., Effect of different preparation methods of MoO_3/Al_2O_3 catalysts on the existing states of Mo species and hydrodesulfurization activity, *Fuel*, Vol. 116, 2014, pp.168-174.

[27] Aleksandrov P. V., Bukhtiyarova G. A., Noskov A. S., Modern approaches to testing granulated catalysts in the hydrotreatment of oil distillates under laboratory conditions. *Catalysis in Industry*, Vol.7, No.1, 2015, pp. 47-53.

[28] Debye P., Scattering from non-crystalline substances, *Ann. Physik.*, Vol. 46, 19 15, pp. 809-823.

[29] Guinier A., *X-ray Diffraction in Crystals, Imperfect Crystals and Amorphous Bodies*, Dover, New York, 1994.

[30] Hall B. D., Debye function analysis of structure in diffraction from nanometer-sized particles, *Journal of Applied Physics*, Vol.87, No.4, 2000, pp. 1666-1675.

[31] Tsybulya S. V., Yatsenko D. A., X-ray diffraction analysis of ultradisperse systems: The Debye formula, *Journal of Structural Chemistry*, Vol.53, No.1, 2012, pp. 150-165.

[32] Yatsenko D. A., Tsybulya S. V., DIANNA (Diffraction Analysis of Nanopowders): Software for structural analysis of ultradisperse systems by X-Ray methods, *Bulletin of the Russian Academy of Sciences: Physics*, Vol.76, No.3, 2012, pp. 382-384.

[33] Nogueira A., Znaiguia R., et al., Curved nanostructures of unsupported and Al_2O_3-supported MoS_2 catalysts: Synthesis and HDS catalytic properties, *Applied Catalysis A-General*, Vol.429, 2012, pp. 92-105.